Development and Performance Evaluation of a Hydrogel Microneedle Sensor for In Situ Monitoring of Potassium Ions in Rice Plants

Jiuxiang Li
Jiangxi Agricultural University
Jinhui Zhao
zhaojh@jxau.edu.cn
Jiangxi Agricultural University
Junshi Huang
Jiangxi Agricultural University
Muhua Liu
Jiangxi Agricultural University
Shuanggen Huang
Jiangxi Agricultural University

Research Article

Keywords: Potassium ion, Real-time detection, Electrochemical sensing, Hydrogel microneedle sensor

Posted Date: January 7th, 2026

DOI: https://doi.org/10.21203/rs.3.rs-8483124/v1

Additional Declarations: No competing interests reported.

Version of Record: A version of this preprint was published at Microchimica Acta on January 31st, 2026.
See the published version at https://doi.org/10.1007/s00604-026-07900-3.

Development and Performance Evaluation of a Hydrogel Microneedle Sensor for In Situ Monitoring of Potassium Ions in Rice Plants

Jiuxiang Li[1,2] · Jinhui Zhao[1] · Junshi Huang[1] · Muhua Liu[1] · Shuanggen Huang[1]

Abstract

The dynamic balance of potassium ions (K^+) in rice plants is critical to their growth, development, and stress res istance. To achieve in-situ, real-time monitoring of K^+ levels in rice plants and overcome the limitations of traditi onal destructive sampling methods, this study developed a biosensor based on ion-selective hydrogel microneedles. Key performance parameters of the sensor, including its calibration curve and sensitivity, were systematically eva luated via in vitro electrochemical tests. Meanwhile, the mechanical strength and microstructure of the microneedl es were characterized using micro-force testing. The practical applicability of the sensor was validated through ag arose gel recovery experiments and in vivo K^+ monitoring in rice plants under salt stress, with results cross-valid ated against ion chromatography as a reference method. The sensor exhibited a sensitivity close to the Nernstian response (59.0 ± 0.11 mV/decade), a linear detection range of 10^{-4} to 10^{-1}M, and a detection limit of 3.0×10^{-5}M. It also demonstrated a fast response time (T_{95} < 20s), excellent stability, and high batch-to-batch reproducibility (r elative standard deviation, RSD < 0.2%). The microneedles achieved a mechanical strength of 25 mN, which is well above the threshold required for penetrating the rice plant epidermis. During in vivo testing, the sensor succ essfully tracked the rapid K^+ loss in rice leaves under salt stress, showing a strong correlation with the standard method (R^2= 0.985). In conclusion, the developed hydrogel microneedle sensor is a stable, reliable, and effective tool for in-situ K^+ analysis in rice plants, providing valuable insights into plant ion physiology and the mechanis ms underlying responses to environmental stress.

Keywords Potassium ion· Real-time detection· Electrochemical sensing· Hydrogel microneedle sensor

Jinhui Zhao

zhaojh@jxau.edu.cn

[1] Jiangxi Agr Univ, Key Lab Modern Agr Equipment Jiangxi Prov, Nanchang 330045, China

[2] Jiangxi Biotech Vocational College,Nanchang 330045, China

Introduction

According to the Food and Agriculture Organization o f the United Nations, increasing global food productio n is essential to feed a growing population, which is projected to reach 7 billion by 2050[1]. Rice stands a s one of the world's most vital staple food crops. Pot assium ions (K^+) are essential macronutrients required for rice growth and development[2]. They play a crit ical role in various physiological processes, including cellular osmotic regulation, enzyme activity modulation, growth regulation, maintenance of membrane potentia l, and pH homeostasis[3]. As the most abundant catio n in rice plants, potassium can account for 2-10% of the dry weight of plant tissues. Within rice cells, the vacuolar K+ concentration typically ranges between 12 0-250mM, while the cytosolic K+ concentration remai ns relatively lower, at approximately 100mM.Potassium deficiency in rice leads to stunted growth and reduce d crop yield[4].

Conventional methods for analyzing ion dynamics i n plants, such as atomic absorption spectroscopy and i on chromatography, typically necessitate destructive tis

sue sampling and complex pretreatment processes[5]. These approaches not only fail to facilitate in-situ, real-time monitoring but also disrupt the spatiotemporal continuity of ion signals, thereby complicating the capture of rapid ion flux events that occur during the early stages of stress responses[6].

In recent years, advancements in micro-nano sensor technology have opened new avenues for research in plant physiology[7]. Among these innovations, microneedle sensors—characterized by their miniature size and low invasiveness—show considerable promise as "artificial trichomes" capable of penetrating the plant epidermis to enable direct, in-situ monitoring of target ions within tissue fluids. However, existing rigid microneedles often induce mechanical stress on soft plant tissues and generally lack selectivity for specific ions. Hydrogel materials are recognized for their excellent biocompatibility, flexibility, and hydrophilic three-dimensional network structures[8]; thus they are considered an ideal matrix for immobilizing ionophores and fabricating ion-selective sensors. Nevertheless, integrating hydrogel with microneedle architectures to develop sensors suitable for in-planta ion monitoring presents significant challenges—particularly regarding the balance between mechanical strength, electrochemical performance, and biocompatibility[9], [10].

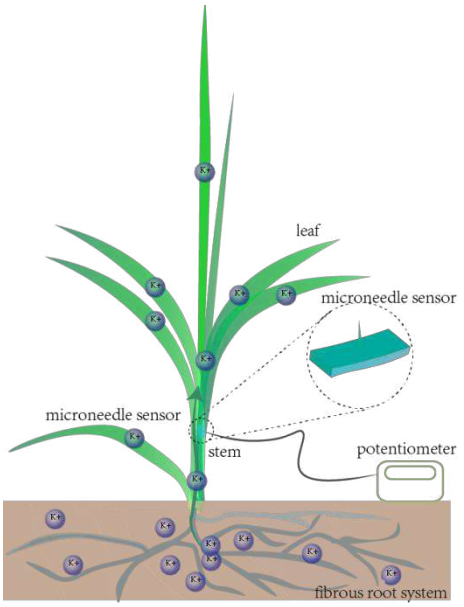

Fig.1 In-vivo potassium ion online monitoring system for rice

This study aims to develop a hydrogel-based microneedle sensor that combines robust mechanical strength with high selectivity for K^+ ions to facilitate in-situ monitoring within plants(Figure 1). We will systematically characterize the sensor's electrochemical performance under controlled laboratory conditions alongside its mechanical properties and microstructure analysis. Ultimately, through simulated environments coupled with in vivo plant experiments, we will validate its accuracy and reliability under complex physiological conditions. We anticipate that this sensor will serve as a powerful tool to elucidate the mechanisms underlying ion transport in plants as well as their dynamic responses to environmental stimuli.

Experimental Section

Materials and Equipment

The chemical reagents used in the experiments included:Gelatin Methacryloyl (GelMA), 2-Hydroxy-2-methylpropiophenone, Phosphate Buffered Saline (PBS), PDMS Microneedle Array Mold, Trichloro(1H,1H,2H,2H-perfluorooctyl)silane, PEDOT:PSS Aqueous Dispersion, Dimethyl Sulfoxide (DMSO), (3-Glycidyloxypropyl)trimethoxysilane, Anhydrous Ethanol, Chloroauric Acid, Potassium Chloride, Poly(vinyl chloride) (PVC), o-Nitrophenyl Octyl Ether (o-NPOE), Lasalocid (Potassium Ionophore I), Sodium Ionophore X, Potassium Tetrakis (3,5-bis (trifluoromethyl) phenyl) borate,Tetrahydrofuran(THF), Poly(sulfobetaine methacrylate) (PSBMA), Polyimide Film, Silver Conductive Adhesive, UV-Curable Adhesive, Medical-Grade Silicone Elastomer, and Biocompatible Hydrocolloid Dressing.

The instruments and equipment employed in the experiments included:Analytical Balance, Magnetic Stirrer/Hot Plate, Ultrasonic Cleaner/Cell Disruptor, Spin Coater, UV Curing Chamber, Vacuum Drying Oven, Plasma Cleaner, Freeze Dryer, Three-Dimensional Precision Mobile Platform with Microinjection Pump, Stereo Microscope/Metallurgical Microscope, Electrochemical Workstation, Reference Electrode, Scanning Electron Microscope (SEM), High-Impedance Potentiometer/Source Meter, and Digital Multimeter.

Fabrication of Hydrogel Microneedles

This study selected methacrylated gelatin (GelMA), a biocompatible material with suitable mechanical strength, as the matrix for the microneedle sensor（Figure 2）. The fabrication process began with the preparation and silanization of a polydimethylsiloxane (PDMS)

mold. A silicon microneedle master mold, fabricated via photolithography and etching techniques, was used as the template. The PDMS prepolymer and curing agent were thoroughly mixed at a 10:1 weight ratio, degassed, and then poured onto the silicon master mold. Curing was carried out at 75℃ for 2 hours. After cooling, the solidified PDMS mold was carefully peeled off from the master.

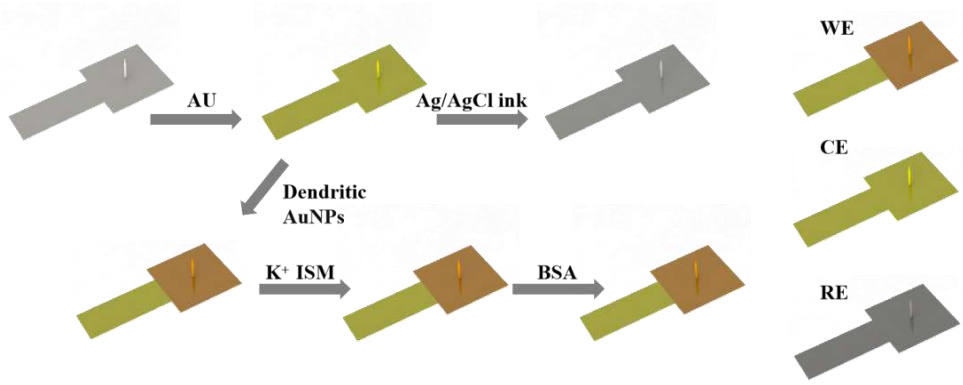

Fig. 2 Flowchart of potassium ion microneedle sensor preparation

Firstly, the PDMS mold was placed inside a vacuum desiccator along with a small petri dish containing 50μL of trichloro (1H,1H,2H,2H-perfluorooctyl) silane. The desiccator was evacuated and maintained under vacuum for 30 minutes to allow the silane vapor to uniformly deposit onto the surface of the PDMS mold.

Secondly, a measured quantity of GelMA powder was dissolved in phosphate-buffered saline (PBS) at 60℃ to prepare a 20–30% (w/v) solution. After the solution cooled to room temperature, 0.5% (w/v) photoinitiator was added, and the mixture was magnetically stirred in the absence of light until complete dissolution was achieved. The prepolymer solution was then placed in a vacuum desiccator for 10-15 minutes to thoroughly remove air bubbles.

Thirdly, the PDMS microneedle mold was positioned horizontally. Using a pipette, the degassed GelMA prepolymer solution was carefully dispensed onto the mold surface, ensuring complete coverage with a slight excess. The entire assembly was then transferred to a centrifuge and spun at 3000-4000 rpm for 20-30 minutes. Centrifugal force facilitated the complete filling of the prepolymer solution into the microneedle cavities, particularly toward the tips. Following centrifugation, a scraper was used to gently remove any excess solution from the mold surface. Finally, the mold was placed in a UV curing chamber and exposed to 365 nm wavelength light for 60–90 seconds to achieve complete cross-linking and solidification of the GelMA.

Finally, the cured hydrogel microneedle array was carefully peeled away from the PDMS mold. The array was then either immersed in PBS for swelling equilibrium or subjected to freeze-drying for long-term storage.

Preparation of Microneedle Biosensors

PEDOT:PSS hydrogel microneedles serve as the counter electrode for microneedle sensors. The PVB/PEDOT:PSS obtained by dropwise coating the PVB-based reference film on the needle tip was used as the reference electrode of the microneedle sensor. The PEDOT:PSS hydrogel microneedles modified by aptamers are used as the working electrodes of the microneedle sensor. The preparation process of the working electrode is shown in Figure 2.

First, the hydrated GelMA microneedle array was subjected to gradient dehydration by sequentially immersing it in 50%, 75%, 95%, and 100% ethanol for 15 minutes each. The dehydrated array was then fixed onto a three-dimensional precision mobile platform. Using a microinjection pump equipped with a hollow glass capillary, the PEDOT:PSS precursor solution was drawn. Under microscopic guidance, the capillary tip was precisely positioned at the tip of an individual microneedle. Approximately 50 nL of the solution was injected at an extremely low flow rate (e.g., 10 nL/s). Relying on capillary action, the solution diffused bac

kward from the needle tip toward the base. The injected microneedle array was then transferred to a hot plate and heated at 60℃ for 30 minutes. The electrical resistance of a single microneedle, measured from its tip to the conductive pad at the base, was tested using a multimeter. A successful preparation was indicated by a stable resistance reading within the range of 1-5 kΩ.

Secondly, using this conductive microneedle as the working electrode, deposition was carried out in a 0.1 m KCL solution containing 0.5mM chloroauric acid for 30 seconds at -0.8V (vs.Ag/AgCl) using the timing amperometric method. At this point, Au^{3+} is reduced to Au^{0}, forming nano-gold clusters with high specific surface area on the surface of PEDOT:PSS. Place the microneedle array in a petri dish saturated with THF vapor (to prevent THF from evaporating too quickly). Using a micropipette, precisely apply approximately 100nL of ISM solution to the tip area under a microscope. Cover the lid and let the film slowly evaporate overnight (>12 hours) in a high-humidity and undisturbed environment.

Again, prepare a solution containing 2.0wt% polysulfonyl betaine methacrylate and 0.5wt%Irgacure2959. Apply a small amount of this solution to the ISO-modified tip area with a fine brush or dispenser. Local irradiation with 365nm ultraviolet light for 20 seconds forms a strong and highly hydrophilic anti-fouling network.

Finally, serpentine conductive traces made of gold or copper were fabricated on a 25μm thick polyimide film using photolithography-etching or laser direct writing techniques. The serpentine design enables stretching and bending compliance. A small droplet of UV-curable biocompatible adhesive was applied to the contact pad of the flexible circuit. The conductive base area of the hydrogel microneedle was carefully aligned and pressed onto the adhesive-coated pad. Localized UV irradiation was then performed through the polyimide film side to cure the adhesive, establishing a robust mechanical and electrical connection. The wire bonding sites and the base of the hydrogel microneedle were fully encapsulated using a medical-grade silicone elastomer, leaving only the functionalized needle tips and the distal connector exposed. A biocompatible hydrocolloid dressing was applied to the backside of the device to serve as an interface for secure attachment to plant stems or leaves.

Results and Discussion

In Vitro Electrochemical Performance of the Sensor

To evaluate the quantitative detection capability of the fabricated hydrogel microneedle sensor for K^+, its potentiometric response was first tested in standard KCl solutions (ranging from 10^{-5} M to 1 M) with a background of 0.1 mM $CaCl_2$. As shown in Figure 3, the electromotive force (EMF) of the four sensors exhibited a strong linear relationship with the negative logarithm of K^+ activity (pK) across the concentration range of 10^{-4} M to 10^{-1} M. Fitting the linear region yielded calibration slopes of 59.18 mV/decade (R^2 = 0.9992), 59.19 mV/decade (R^2 = 0.9993), 59.16 mV/decade (R^2 = 0.9992), and 59.22 mV/decade (R^2 = 0.9992). These values are all in excellent agreement with the theoretical Nernstian response at 25°C (59.2 mV/decade), indicating that the ion-exchange process within the sensor membrane is near-ideal and demonstrates excellent sensitivity. The linear range spans four orders of magnitude, from 10^{-4}M to 10^{-1}M, which is sufficient to cover the physiological fluctuation range of K^+ concentrations in plants. At 10^{-5}M, the potential value deviated significantly below the linear extrapolation, allowing the limit of detection to be reported as $<1\times10^{-4}$M. This ensures reliable detection in low-concentration environments.

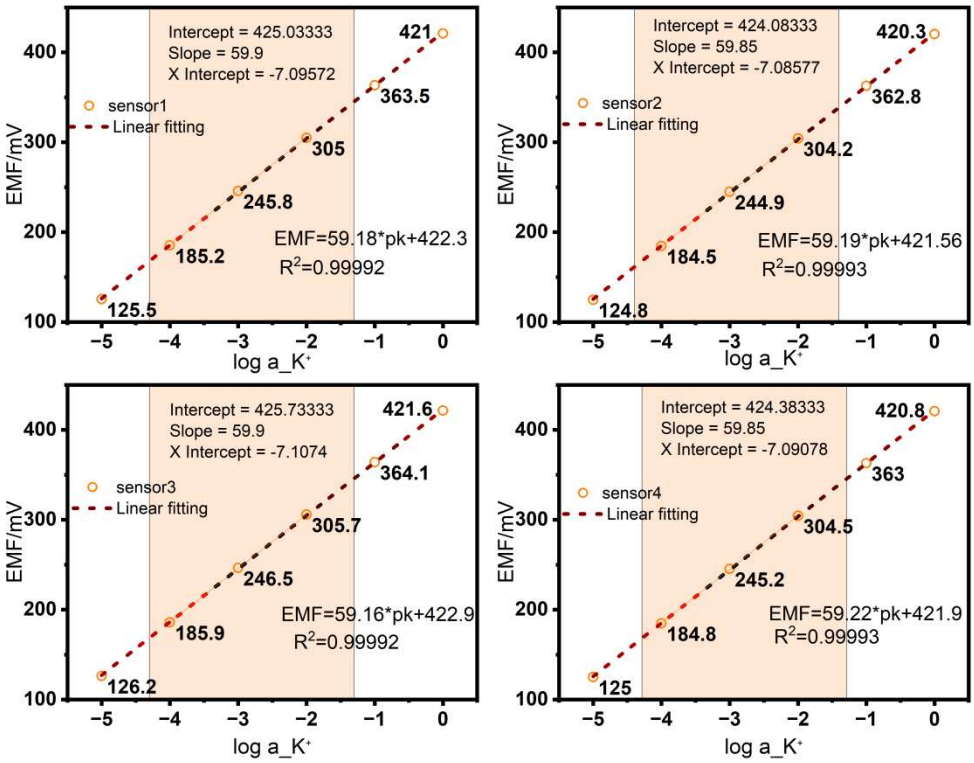

Fig. 3 The relationship between the electromotive force (EMF) of the four sensors and the logarithm of K^+ activity (pK)

Selectivity is a critical factor determining the sensor 's accuracy in complex physiological environments. Th e fixed interference method (FIM) was employed to e valuate the sensor's anti-interference capability against common coexisting ions (Na^+, Ca^{2+}, NH_4^+, H^+). As sh own in Figure 4a, when the Na^+ concentration was fi xed at 1 mM, the calibration curve for K^+ began to deviate at K^+ concentrations below 1×10^{-3} M. The calculated selectivity coefficient was log K_{pot}^{K, Na} ≈ 0. This value indicates that the sensor exhibits a preference for K^+ over Na^+, though it still deviates slightly from the ideal value (<<0), which may be a ttributed to weak non-specific adsorption of Na^+ by th e hydrogel matrix. Nevertheless, in typical plant tissue s, the K^+ concentration is generally much higher than that of Na^+, making this level of selectivity sufficien t for most application scenarios. For other interfering ions (e.g., Ca^{2+}, H^+), the calculated log K_{pot} value s were all below -1.5, demonstrating excellent anti-int erference capability against these ions.

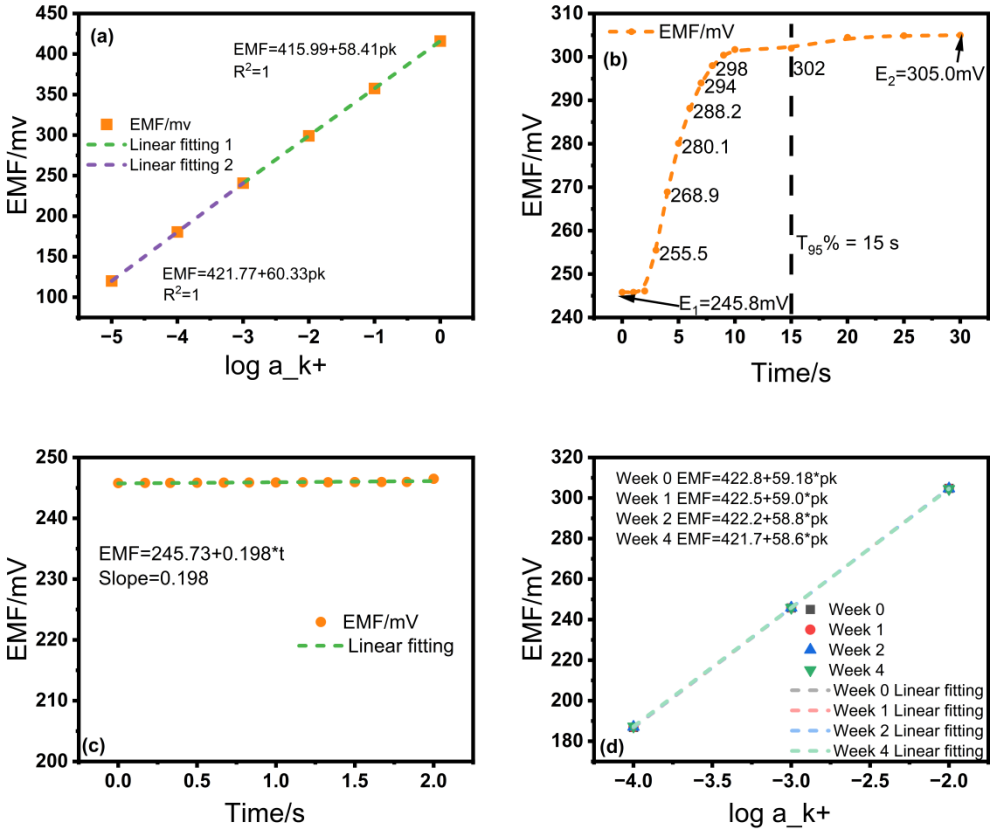

Fig.4 Selectivity, Response Time, and Stability of the Potassium Ion Sensor

Response time is crucial for monitoring dynamic changes in ion concentrations within plants. As shown in Figure 4b, when the sensor was transferred from a 10^{-3}M KCl solution to a 10^{-2}M solution, the potential reached 95% of its steady-state value (T_{95}%) within 15 seconds. This rapid response is attributed to the micrometer-scale dimensions and hydrophilic porous structure of the hydrogel microneedle, which significantly facilitate fast ion diffusion and transport, enabling the sensor to capture transient changes in ion concentration.

Stability test results (Figure 4c) demonstrated excellent short-term stability, with a potential drift rate of only 0.35 mV/h during continuous testing in 1 mM KCl solution for 2 hours. Furthermore, a four-week long-term stability study (Figure 4d) revealed that the sensor's sensitivity gradually decreased from an initial value of 59.18 mV/decade to 58.6 mV/decade, representing a change of less than 0.98%. This minimal attenuation is well below commonly accepted thresholds, indicating outstanding long-term stability. The slight performance degradation may be related to minor leaching of the ionophore from the hydrogel or aging of the membrane. Nevertheless, over a one-month period, the sensor maintained sufficiently stable performance to reliably complete a series of experiments.

Reproducibility and Repeatability

To ensure the reliability of detection results, the sensor's reproducibility and repeatability were quantitatively evaluated. The relative standard deviation (RSD) of the electromotive force (EMF) measured from five independently fabricated sensors of the same batch in 1 mM KCl standard solution was 0.38% (Figure 5a). This exceptionally low batch-to-batch variation demonstrates the high reproducibility of the microfabrication and hydrogel preparation processes employed, which is advantageous for large-scale production and standardized applications. Furthermore, when a single sensor was used to perform five repeated measurement-rinsing cycles in 1 mM KCl solution, the RSD was as low as 0.12% (Figure 5b). This result confirms the excellent operational repeatability of individual sensors, ensuring data comparability and accuracy during continuous monitoring. The robust mechanical structure of the microneedles and the stable electrochemical properties

of the hydrogel membrane are key factors contributin g to this high repeatability.

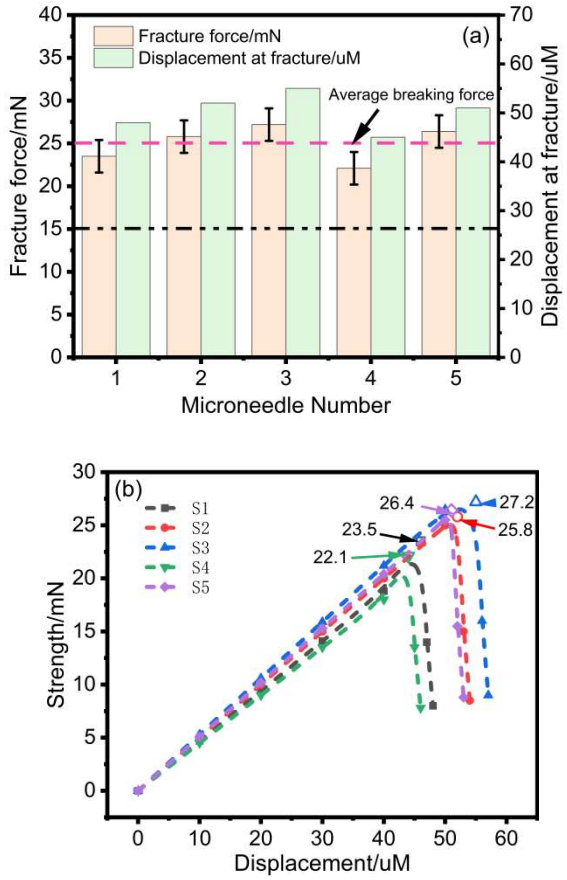

Fig.5 force-displacement curve characteristics

Mechanical Properties

To ensure the successful application of the microneedl e sensor in plants and the acquisition of reliable sign als, its mechanical strength and structural morphology were systematically characterized. First, compression tests were performed on individual microneedles using a microforce tester. The results, shown in Figure 5a, revealed typical brittle fracture characteristics in the force-displacement curve, with an average fracture for ce of 25.3 ± 2.1 mN (n = 5). According to literature reports, successful penetration of the epidermis of co mmon plant leaves such as Arabidopsis and tobacco r equires only about 5–15 mN of force. The mechanica l strength of our sensor is significantly higher than th is threshold, indicating a high safety margin during in sertion and effectively preventing experimental failure due to needle tip bending or fracture.

Practical Application Performance Evaluation

Accuracy Validation in a Tissue Simulant.To evaluate the detection accuracy of the sensor in a plant tissue-like environment, a recovery test was conducted by in serting it into a 1% (w/v) agarose gel containing a k nown K^+ concentration (5.0 mM). The measured K^+ c oncentration was 4.9±0.2 mM (n=3), yielding a high recovery rate of 98.0%(Figure 6a). This near-quantita tive recovery demonstrates that the sensor's detection performance remains largely unaffected by diffusion li mitations or matrix effects, even in a gel environment simulating the plant intercellular space, highlighting i ts accurate quantitative capability in complex three-di mensional systems.

Dynamic Monitoring and Validation in Living Plant s.During the early stage of salt stress, the sensor succ essfully captured a sharp decrease in K^+ concentration within the leaf (Figure 6b). This observation is highl y consistent with the known physiological response to salt stress: the influx of high concentrations of Na^+ disrupts ionic homeostasis, often triggering the efflux of K^+ through non-selective cation channels. Our sens or recorded this critical physiological process in real t ime, highlighting its unique advantage in providing hi gh spatiotemporal resolution for studying plant stress r esponses.

To rigorously validate the accuracy of the sensor d ata in a living plant environment, we employed ion c hromatography (IC) as a standard reference method fo r comparative analysis. Under identical salt stress con ditions, leaf samples were collected at different time points, and the K^+ concentration was measured using both our sensor and the IC method. As shown in Fig ure 6b, the results obtained from the two methods de monstrated excellent agreement, with a linear regressio n of: $[K^+]\_sensor = 0.98 \times [K^+]\_IC + 0.05$ ($R^2 = 0.9$ 85). The slope of the fitted line is close to 1, the int ercept is near 0, and the coefficient of determination (R^2) exceeds 0.98, strongly demonstrating that our mic roneedle sensor can provide highly accurate quantitativ e information even within the real and complex intern al environment of plants.

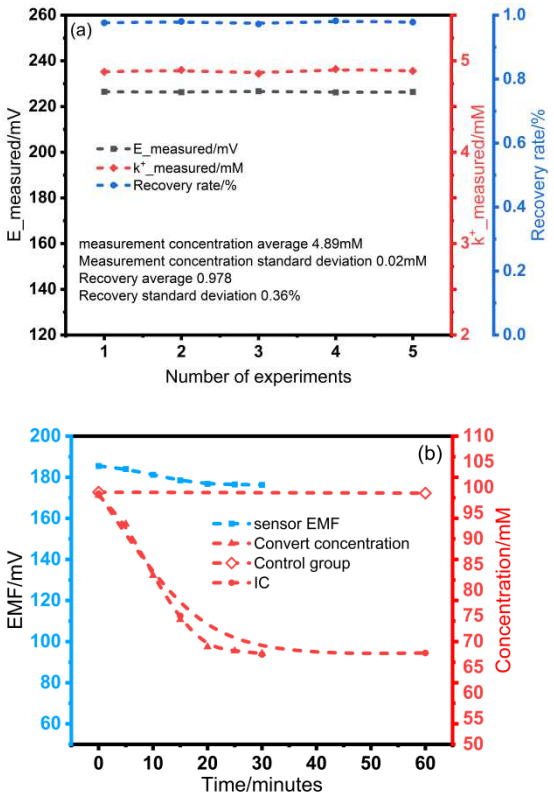

Fig.6 Evaluate the detection accuracy of the sensor in a plant-like tissue environment

Conclusions

Based on the comprehensive research presented above, we have successfully developed and systematically evaluated a hydrogel microneedle sensor for detecting K^+ in plants. In vitro electrochemical tests confirmed its high sensitivity, excellent selectivity, fast response, and good stability. Mechanical characterization demonstrated that it possesses sufficient structural strength to penetrate the plant epidermis. Ultimately, through experiments in tissue simulants and living plants, we not only validated the accuracy of its detection results but also captured, for the first time, the dynamic decrease of K^+ concentration in tobacco leaves during the early stage of salt stress in situ and in real time. This sensor combines the low invasiveness of microneedles with the excellent biocompatibility and ion conductivity of hydrogels, providing a powerful tool for plant physiology research, particularly in areas such as dynamic ion transport and stress response mechanisms. Future work will focus on developing integrated microneedle arrays for the simultaneous detection of multiple ions (e.g., K^+, Na^+, H^+) and exploring their application in a wider range of plant species and more complex field environments.

Funding The authors gratefully acknowledge the financial support from the Science and Technology Research Project of the Jiangxi Provincial Department of Education (Grant No. GJJ250726)

Data availability The data available within the article or its supple- mentary materials.

References

[1] Q. Wang, Á. Molinero-Fernández, J. Acosta-Motos, G. Crespo, and M. Cuartero, "Unveiling potassium and sodium ion dynamics in living plants with an in-planta potentiometric microneedle sensor," *ACS Sens.*, vol. 9, pp. 5214–5223, 2024, doi: 10.1021/acssensors.4c01352.

[2] L. Liu, H. Kai, K. Nagamine, Y. Ogawa, and M. Nishizawa, "Porous polymer microneedles with interconnecting microchannels for rapid fluid transport," *RSC Adv.*, vol. 6, no. 54, pp. 48630–48635, 2016, doi: 10.1039/C6RA07882F.

[3] Z. Li *et al.*, "A potassium ion sensor with an acupuncture needle inserted into a glass capillary for small-volume sample detection," *MICROCHEMICAL JOURNAL*, vol. 213. ELSEVIER, RADARWEG 29, 1043 NX AMSTERDAM, NETHERLANDS, June 2025. doi: 10.1016/j.microc.2025.113870.

[4] D. Ai, X. Tang, Z. Meng, Y. Yu, X. Guo, and Y. Wang, "Porous microneedle-based electrochemical sensor for potassium and glucose in skin interstitial fluid," *ANALYTICAL METHODS*, vol. 17, no. 37. ROYAL SOC CHEMISTRY, THOMAS GRAHAM HOUSE, SCIENCE PARK, MILTON RD, CAMBRIDGE CB4 0WF, CAMBS, ENGLAND, pp. 7541–7550, Sept. 25, 2025. doi: 10.1039/d5ay00915d.

[5] K. Liu *et al.*, "Flexible and wearable sensor for in situ monitoring of gallic acid in plant leaves," *FOOD CHEMISTRY*, vol. 460, no. 3. ELSEVIER SCI LTD, 125 London Wall, London, ENGLAND, Dec. 01, 2024. doi: 10.1016/j.foodchem.2024.140740.

[6] Q. Wei *et al.*, "Wearable 3D-printed microneedle sensor for intradermal temperature monitoring," *ACS SENSORS*, vol. 10, no. 6. AMER CHEMICAL SOC, 1155 16TH ST, NW, WASHINGTON, DC 20036 USA, pp. 4027–4037, Apr. 15, 2025. doi: 10.1021/acssensors.4c03681.

[7] S. N. Economidou and D. Douroumis, "3D printing as a

transformative tool for microneedle systems: Recent advances, manufacturing considerations and market potential," *ADVANCED DRUG DELIVERY REVIEWS*, vol. 173. ELSEVIER, RADAR WEG 29, 1043 NX AMSTERDAM, NETHERLANDS, pp. 60–69, June 2021. doi: 10.1016/j.addr.2021.03.007.

[8] F. Inci *et al.*, "Bio-inspired magnetic beads for isolation of sperm from heterogenous samples in forensic applications," *FORENSIC SCIENCE INTERNATIONAL-GENETICS*, vol. 52. ELSEVIER IRELAND LTD, ELSEVIER HOUSE, BROOKVALE PLAZA, EAST PARK SHANNON, CO, CLARE, 00000, IRELAND, May 2021. doi: 10.1016/j.fsigen.2020.102451.

[9] K. Yu *et al.*, "Individually modified microneedle array for minimal invasive multi-electrolyte monitoring," *BIOSENSORS-BASEL*, vol. 15, no. 5. MDPI, MDPI AG, Grosspeteranlage 5, CH-4052 BASEL, SWITZERLAND, May 12, 2025. doi: 10.3390/bios15050310.

[10] X. Dong, M. C. Vuran, and S. Irmak, "Autonomous precision agriculture through integration of wireless underground sensor networks with center pivot irrigation systems," *AD HOC NETWORKS*, vol. 11, no. 7, SI. ELSEVIER, RADARWEG 29, 1043 NX AMSTERDAM, NETHERLANDS, pp. 1975–1987, Sept. 2013. doi: 10.1016/j.adhoc.2012.06.012.

Supplementary Files

This is a list of supplementary files associated with this preprint. Click to download.

- GelsandBlotsimages4.png
- GelsandBlotsimages2.png
- GelsandBlotsimages3.png
- GelsandBlotsimages1.png
- GelsandBlotsimages5.png
- GelsandBlotsimages6.png